cancer cells and tumorigenic hepatic progenitor cells. *Clin Cancer Res* 2009; **15**: 3462–71.
29 Inaba Y, Kanai F, Aramaki T *et al.* A randomized phase II study of TSU-68 in patients with hepatocellular carcinoma treated by transarterial chemoembolization. *Eur J Cancer* 2013; 49: 2832–40.

SUPPORTING INFORMATION

ADDITIONAL SUPPORTING INFORMATION may be found in the online version of this article at the publisher's website:

Figure S1 Relationship between overall survival and platelet-derived growth factor (PDGF)-BB. PDGF-BB concentration had significant positive correlation with neutrophil to lymphocyte ratio (NLR) on the basis of weighted linear regression ($r = 0.227$; $P = 0.035$).

Liver
INTERNATIONAL

Liver International ISSN 1478-3223

NAFLD & NASH

Characteristics of hepatic fatty acid compositions in patients with nonalcoholic steatohepatitis

Kazutoshi Yamada[1], Eishiro Mizukoshi[1], Hajime Sunagozaka[1], Kuniaki Arai[1], Tatsuya Yamashita[1], Yumie Takeshita[2], Hirofumi Misu[2], Toshinari Takamura[2], Seiko Kitamura[3], Yoh Zen[3], Yasuni Nakanuma[4], Masao Honda[1] and Shuichi Kaneko[1]

1 Department of Gastroenterology, Graduate School of Medicine, Kanazawa University, Kanazawa, Japan
2 Department of Disease Control and Homeostasis, Graduate School of Medicine, Kanazawa University, Kanazawa, Japan
3 Division of Pathology, Kanazawa University Hospital, Kanazawa, Japan
4 Department of Human Pathology, Graduate School of Medicine, Kanazawa University, Kanazawa, Japan

Keywords
fatty acid metabolism – insulin resistance – palmitic acid – toxic lipid

Abbreviations
ACC, acetyl-CoA carboxylase; BMI, body mass index; ELOVL6, elongation of long-chain fatty acids family member 6; FAS, fatty acid synthase; HOMA-IR, homoeostasis model assessments of insulin resistance; NAFLD, nonalcoholic fatty liver disease; NASH, nonalcoholic steatohepatitis; NAS, NAFLD activity score; PPAR, peroxisome proliferator-activated receptor; QUICKI, Quantitative Insulin Sensitivity Check Index; SCD, stearoyl-CoA desaturase; SREBP-1c, sterol regulatory element-binding protein-1c; SS, simple steatosis; T-CHO, total cholesterol; TG, triglyceride.

Correspondence
Shuichi Kaneko, Department of Gastroenterology, Graduate School of Medicine, Kanazawa University, Kanazawa, Ishikawa 920-8641, Japan
Tel: +81 76 265 2230
Fax: +81 76 234 4250
e-mail: skaneko@m-kanazawa.jp

Received 9 January 2014
Accepted 3 September 2014

DOI:10.1111/liv.12685
Liver Int. 2015; 35: 582–590

Abstract

Background & Aims: Nonalcoholic fatty liver disease (NAFLD) is closely related to insulin resistance and lipid metabolism. Recent studies have suggested that the quality of fat accumulated in the liver is associated with the development of nonalcoholic steatohepatitis (NASH). In this study, we investigated the fatty acid composition in liver tissue and its association with the pathology in NAFLD patients. *Methods:* One hundred and three patients diagnosed with NAFLD [simple steatosis (SS): 63, NASH: 40] were examined and their hepatic fatty acids were measured using gas chromatography. In addition, relationships between the composition and composition ratios of various fatty acids and patient backgrounds, laboratory test values, histology of the liver, and expression of fat metabolism-related enzymes were investigated. *Results:* The C16:1n7 content, the C16:1n7/C16:0 and C18:1n9/C18:0 ratios were increased and the C18:0/C16:0 ratio was decreased in the NASH group. The C18:0/C16:0 and C18:1n9/C18:0 ratios were associated with the steatosis score in liver tissue, and the C16:1n7/C16:0 ratio was associated with the lobular inflammation score. The expressions levels of genes: SCD1, ELOVL6, SREBP1c, FAS and PPARγ were enhanced in the NASH group. In multivariate analysis, the C18:0/C16:0 ratio was the most important factor that was correlated with the steatosis score. In contrast, the C16:1n7/C16:0 ratio was correlated with lobular inflammation. *Conclusion:* The fatty acid composition in liver tissue and expression of genes related to fatty acid metabolism were different between the SS and NASH groups, suggesting that the acceleration of fatty acid metabolism is deeply involved in pathogenesis of NASH.

The number of patients with nonalcoholic fatty liver disease (NAFLD) has increased in Western countries and Asia, and the increase in obese people and changes in dietary life has become a major health issue (1, 2). NAFLD includes simple steatosis (SS) with a favourable prognosis and nonalcoholic steatohepatitis (NASH). NASH is considered to develop when an exacerbating factor is added to fat deposition in liver tissue, with oxidative stress, inflammatory cytokines and iron-related factor being attributed as causes of NASH (3–5). However, the detailed developmental mechanism for NASH has not been fully elucidated and no evidence-based treatment method has been established, although several drugs have been suggested to be effective (6–8). The prognosis is poor once the condition has progressed to NASH, and the incidence of liver-related death significantly increases with the progression to hepatic cirrhosis. Therefore, identifying factors that con-

tribute to the progression of SS to NASH is vitally important and a treatment method needs to be established to prevent its progression.

Previous studies have clarified that insulin resistance is closely involved in the development of NAFLD (9–11). On the other hand, it has recently been reported that the composition of fatty acids in liver tissue and the expression level of elongation of long-chain fatty acids family member 6 (ELOVL6), which regulates their composition, are factors determining insulin resistance (12), and reducing the activity of fatty acid desaturase, stearoyl-CoA desaturase 1 (SCD1), exacerbates hepatocellular disorders and liver tissue fibrosis (13). These reports have suggested an association between the development of NAFLD or NASH and the amount and composition ratios of fatty acids accumulated in the liver and the expression of enzymes regulating them. In a previous report on liver tissue fatty acids in NAFLD patients, the fatty acid composition was different from that in healthy subjects; however, the number of subjects was small and how these changes were associated with the clinical characteristics of NAFLD was not clarified (14).

Thus, in this study, we measured the fatty acid contents of liver tissue in 103 NAFLD patients, clarified the characteristics of the composition and composition ratio of these fatty acids, and investigated their association with the disease state and pathological changes. In addition, we analysed the gene expression of enzymes involved in fatty acid synthesis and degradation, which influence changes in the liver tissue fatty acid composition, and clarified their roles in the pathogenesis of NAFLD.

Materials and methods

Patients and laboratory testing

The subjects in this study were 103 patients diagnosed with NAFLD based on pathological examinations of liver tissue collected by ultrasound-guided percutaneous liver biopsies at our institution between December 1998 and September 2010. All patients were hepatitis B surface antigen (HBsAg) and hepatitis C virus antibody negative, and the volume of alcohol consumption per day was less than 20 g. A pathological evaluation was independently performed by two pathologists, and diagnoses were made based on Matteoni's classification (15). Types 1 and 2 of this classification were defined as SS and types 3 and 4 were defined as NASH (SS: 63 patients, NASH: 40 patients). In all patients, three items of the NAFLD activity score (NAS; steatosis, lobular inflammation and hepatocellular ballooning) and fibrosis were also scored (16). In addition, 18 patients who underwent hepatectomy or autopsy for other diseases with no fibrosis or fatty changes on pathological examination of the liver or other chronic liver diseases were included as controls. The first biopsy sample was used in patients who underwent liver biopsies multiple times. All patients gave written informed consent to participate in the study in accordance with the Helsinki Declaration and this study was approved by the Regional Ethics Committee (Medical Ethics Committee of Kanazawa University, no. 829).

The blood test findings of patients whose blood was collected in a fasting state on admission for liver biopsy were adopted.

Insulin resistance was evaluated based on homoeostasis model assessments of insulin resistance (HOMA-IR) [fasting serum insulin (μU/ml) × fasting plasma glucose (mg/dl)/405] and the Quantitative Insulin Sensitivity Check Index (QUICKI) [1/log (fasting serum insulin (μU/ml) × fasting plasma glucose (mg/dl)/405] calculated from fasting-state blood glucose and insulin levels. In some patients (20 SS and 15 NASH patients), insulin resistance was also evaluated by performing the hyperinsulinaemic–euglycaemic clamp (17).

Fatty acid extraction

Liver specimens collected by percutaneous liver biopsy or hepatectomy were used. The wet weight of the liver specimen was measured, and fatty acids were extracted as follows: The liver specimen was placed in KOH methanol solution, combined with 100 μl of pentadecanoic acid methanol solution as an internal reference, and saponified by heating at 100°C for 30 min. After acidifying the solution with 1 N aqueous hydrochloric acid solution, fatty acids were extracted by adding hexane as a solvent, followed by methyl esterification using 14% BF3 methanol solution (P/N1022-12002, GL Sciences, Tokyo, Japan).

Measurement and analysis of liver tissue fatty acids

Extracted fatty acids were identified and quantified by gas chromatography using a Shimadzu, Kyoto, Japan Gas Chromatograph GC-2014AF/SPL and Rtx-2330 column. Chromatographs were analysed using GC solution version 2.3. (Shimadzu Corporation, Kyoto, Japan) The external reference method was employed for the identification and quantitative analysis of fatty acids using TM37Component FAME Mix 47885-U of Supelco (Sigma–Aldrich, St. Louis, MO, USA) as a reference solution. The liver tissue fatty acid content was quantified as an amount per 1 mg of wet liver tissue, and differences in the fatty acid content and composition ratio among the Control, SS and NASH groups were investigated. In this study, n-6 fatty acids were calculated by the sum of C18n2n6, 20:3n6 and 20:4n6, while n-3 fatty acids were calculated by the sum of C18:3n3 and C22:6n3. In addition, the association between physical and blood data and the pathological findings of patients with fatty acids were evaluated. To investigate the association of fatty acid-synthesizing enzymes, the substrate: product fatty acid ratio was determined, and differences among the groups and in the pathological characteristics were evaluated.

Quantitative real-time detection-PCR

We performed quantitative real-time detection (RTD)-PCR using TaqMan Universal Master Mix (PE Applied Biosystems, Foster City, CA, USA). Primer pairs and probes for SCD, ELOVL6, SREBF1, FASN, ACACA, PPARA, PPARG and GAPDH were obtained from the TaqMan assay reagent library. Total RNA was isolated from liver tissue samples using an RNA extraction kit (Micro RNA Extraction Kit; Stratagene, La Jolla, CA, USA). We reverse-transcribed 1 μg of isolated RNA to cDNA using SuperScript® II RT (Invitrogen, Carlsbad, CA, USA) according to the manufacturer's instructions, and the resultant cDNA was amplified with appropriate TaqMan assay reagents as previously described (18).

Statistical analysis

Data are expressed as the mean ± SEM. Differences in the clinical features and amount of fatty acids among the three groups consisting of controls, patients with SS and patients with NASH were analysed for significance by Mann–Whitney's *U*-test, Spearman's rank correlation, and single and multiple regression analysis. A level of $P < 0.05$ was considered significant.

Table 1. Characteristics of the study population

Variable	Control (n = 18)	SS (n = 63)	NASH (n = 40)
Gender M/F	10/8	37/26	19/21
Age (years)	62.8 ± 3.9	46.1 ± 1.9*	52.2 ± 2.7*
Height (cm)	160.1 ± 2.5	162.2 ± 1.3	160.5 ± 1.6
Weight (kg)	53.7 ± 2.3	75.6 ± 2.6*	77.0 ± 2.9*
BMI (kg/m²)	20.9 ± 0.7	28.7 ± 0.8*	29.7 ± 0.8*
AST (IU/L)	32.9 ± 7.2	35.3 ± 5.7	56.9 ± 4.6*,†
ALT (IU/L)	32.2 ± 5.8	58.4 ± 11.6*	82.0 ± 7.3*,†
PLT (×10⁴/mm³)	22.6 ± 1.8	24.0 ± 0.9	20.3 ± 1.1
Total Protein (g/dl)	6.5 ± 0.3	7.0 ± 0.1*	7.1 ± 0.1*
Albumin (g/dl)	3.3 ± 0.2	4.4 ± 0.1*	4.21 ± 0.1*,†
PT (%)	77.9 ± 4.2	97.8 ± 1.7*	97.2 ± 2.7*
HbA1c (%)	5.8 ± 0.3	7.1 ± 0.2*	7.1 ± 0.3*
HOMA-IR	–	3.8 ± 0.5	7.2 ± 1.3*,†
QUICKI	–	0.33 ± 0.0	0.30 ± 0.0†
GIR (mg/kg/min)	–	5.9 ± 0.6	4.3 ± 0.3†
Total cholesterol (mg/dl)	165.5 ± 11.7	201.2 ± 5.2*	193.9 ± 5.7*
Triglycerides (mg/dl)	90.1 ± 9.5	135.4 ± 9.3*	153.6 ± 15.2*
HDL cholesterol (mg/dl)	43.2 ± 4.2	46.1 ± 1.2	49.0 ± 2.2
LDL cholesterol (mg/dl)	107.9 ± 10.6	127.8 ± 4.9	115.6 ± 5.1

The data are expressed as the mean ± SEM.
ALT, alanine aminotransferase; AST, aspartate aminotransferase; GIR, glucose infusion rate.
*$P < 0.05$ vs. the control.
†$P < 0.05$ vs. SS.

Results

Patient profiles

The backgrounds of patients in the Control, SS and NASH groups are shown in Table 1. The mean age of the patients was 50.6 years, and the male: female ratio was 66:55. No significant difference was observed in the use of medications for dyslipidaemia and diabetes between the SS and NASH groups. The body mass index (BMI), haemoglobin A1c (HbA1c) value, and total cholesterol (T-CHO) and triglyceride (TG) levels were significantly higher in the SS and NASH groups than in the Control group. Aspartate aminotransferase and alanine

Table 2. Histopathological findings of livers in the study population

	SS	NASH	*P*-value
Fibrosis (0/1/2/3/4)	7/52/4/0/0	1/15/11/7/6	< 0.01
Steatosis (0/1/2/3)	0/30/24/9	0/10/15/15	< 0.01
Lobular inflammation (0/1/2/3)	6/34/23/0	0/8/26/6	< 0.01
Hepatocellular ballooning (0/1/2)	41/21/1	1/17/22	< 0.01

Table 3. Fatty acid composition in liver tissue of the study population

	Control (n = 18)	SS (n = 63)	NASH (n = 40)
C12:0	0.25 ± 0.10	10.9 ± 2.3*	14.4 ± 3.5*
C14:0	2.4 ± 0.5	36.9 ± 5.1*	67.2 ± 1.4*
C16:0	54.5 ± 6.7	528 ± 80.3*	928 ± 210*
C16:1n7	5.6 ± 1.0	58.3 ± 10.6*	109 ± 23.5*,†
C17:0	3.4 ± 1.8	15.6 ± 2.4*	20.3 ± 3.9*
C18:0	33.6 ± 4.9	162 ± 24.3*	210 ± 40.4*
C18:1n9	36.0 ± 4.8	616 ± 110*	1036 ± 234*
C18:2n6	36.2 ± 3.9	270 ± 46.5*	387 ± 75.7*
C20:1n9	1.0 ± 0.3	18.1 ± 3.3*	24.7 ± 4.4*
C18:3n3	0.4 ± 0.1	6.0 ± 1.0*	9.1 ± 1.9*
C22:1n9	19.1 ± 2.7	56.3 ± 7.8*	57.6 ± 9.5*
C22:2n6	3.08 ± 0.6	10.9 ± 1.5*	10.9 ± 1.5*
C22:6n3	21.7 ± 3.7	54.2 ± 6.8*	51.2 ± 6.8*
C18:0/C16:0 ratio	0.62 ± 0.02	0.35 ± 0.01*	0.27 ± 0.01*,†
C16:1n7/ C16:0 ratio	0.10 ± 0.01	0.10 ± 0.00	0.13 ± 0.01†
C18:1n9/ C18:0 ratio	1.17 ± 0.12	3.43 ± 0.20*	4.22 ± 0.19*,†
n-6/n-3	2.18 ± 0.24	4.21 ± 0.26*	5.25 ± 0.38*,†

The data are expressed as 10^{-4} mg/mg liver, the mean ± SEM.
Lauric acid (C12:0), myristic acid (C14:0), palmitic acid (C16:0), palmitoleic acid (C16:1n7), heptadecanoic acid (C17:0), stearic acid (C18:0), oleic acid (C18:1n9), linoleic acid (C18:2n6), gondoic acid (C20:1n9), α-linolenic acid (C18:3n3), erucic acid (C22:1n9), docosadienoic acid (C22:2n6), docosahexaenoic acid (C22:6n3).
*$P < 0.05$ vs. the control.
†$P < 0.05$ vs. SS.

aminotransferase were significantly higher, and the platelet count and albumin level were significantly lower in the NASH group than in the SS group. HOMA-IR, QUICKI and the glucose infusion rate were significantly different between the groups, with insulin resistance being significantly higher in the NASH group.

The histopathological findings of livers are shown in Table 2. The progression of steatosis, inflammation, hepatocellular disorders and fibrosis was significantly further in the NASH group than in the SS group.

Comparison of the fatty acid content of liver tissue

The fatty acids shown in Table 3 were measured in extracts from liver tissue using gas chromatography. When the fatty acid content per 1 mg of wet liver was compared, various fatty acid contents were significantly higher in the SS and NASH groups than in the control group ($P < 0.05$). In addition, the palmitoleic acid (C16:1n7) content was significantly higher in the NASH group than in the SS group ($P < 0.05$).

Regarding the fatty acid composition ratio, the stearic acid (C18:0)/palmitic acid (C16:0) ratio was significantly lower ($P < 0.01$) and the C16:1n7/C16:0 and oleic acid (C18:1n9)/C18:0 ratios were significantly higher in the NASH group than in the SS group ($P < 0.01$). Differences in the fatty acid composition ratio between the SS and NASH groups were more prominent in men, while no significant difference was noted in premenopausal women (Table S1). The n-6/n-3 ratio was significantly higher in the NASH group than in the SS group ($P < 0.05$). (Table 3)

Fatty acid composition ratio and insulin resistance

The association between the fatty acid composition ratio in liver tissue and insulin resistance was investigated. For the indices of insulin resistance, HOMA-IR and QUICKI calculated from the fasting-state blood glucose and insulin levels were used. Firstly, patients were divided into two groups with (>2.5) and without (≤2.5) insulin resistance based on HOMA-IR. The C18:0/C16:0 ratio was significantly lower and that of the C18:1n9/C18:0 ratio was significantly higher in the group with insulin resistance ($p < 0.01$ and $p = 0.01$, respectively) (Fig. 1A), whereas no significant difference was noted in the C16:1n7/C16:0 ratio between the groups. Similarly, when patients were divided into two groups with (≤0.33) and without (>0.33) insulin resistance based on the QUICKI, the C18:0/C16:0 ratio was significantly lower and the C18:1n9/C18:0 ratio was significantly higher in the group with insulin

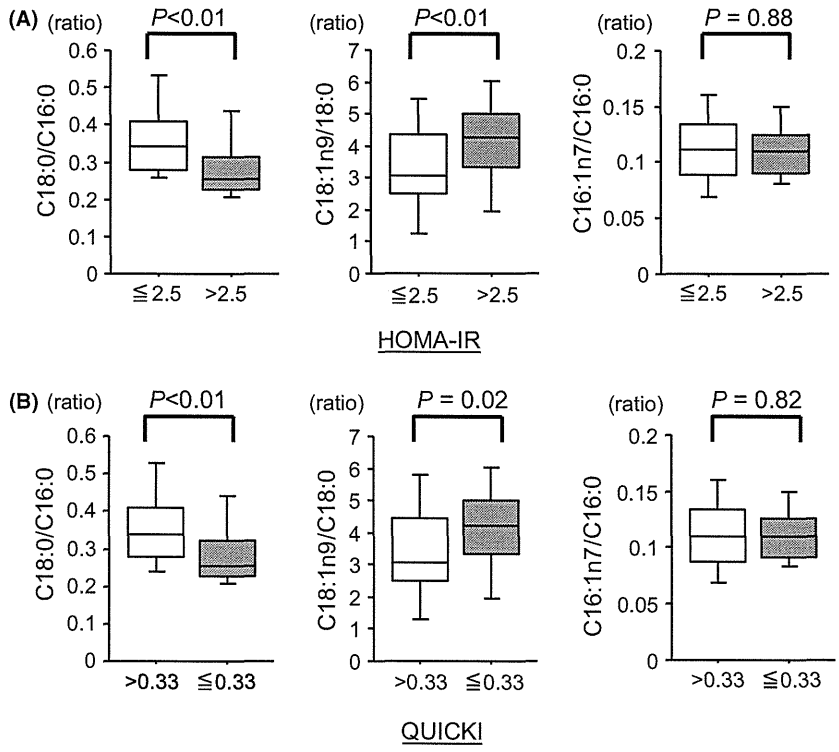

Fig. 1. Association between insulin resistance and the fatty acid composition ratio in liver tissue. The association between insulin resistance and changes in the fatty acid composition ratio in liver tissue was analysed using the Mann–Whitney *U*-test. (A) Patients were divided into groups with and without insulin resistance based on the Homoeostasis Model Assessment for insulin resistance (HOMA-IR) >2.5 as insulin-resistant. (B) Patients were divided into groups with and without insulin resistance based on the QUICKI <0.33 as insulin-resistant.

resistance ($P < 0.01$ and $P = 0.02$, respectively) (Fig. 1B), whereas the C16:1n7/C16:0 ratio showed no association with the presence or absence of insulin resistance.

Fatty acid composition ratio and histopathological findings of the liver

The histopathological findings of the liver with NAFLD were evaluated based on four evaluation items (three items of NAS: steatosis, lobular inflammation, hepatocellular ballooning, and liver fibrosis), and their associations with the liver tissue fatty acid composition ratio were investigated. On evaluation of the association between the NAS and fatty acid composition ratio, the C18:0/C16:0 ratio was significantly lower ($P < 0.01$) and the C18:1n9/C18:0 and C16:1n7/C16:0 ratios were significantly higher ($P < 0.01$) in the group with a 4 or lower score than in the group with a 5 or higher score, showing differences similar to those between the SS and NASH groups (Fig. 2A). Regarding fatty changes (steatosis score), various fatty acid contents significantly increased with an increase in the score. A significant decrease in the C18:0/C16:0 ratio ($P < 0.01$) and a significant increase in the C18:1n9/C18:0 ratio ($P < 0.01$) were noted in the fatty acid composition, but no association with the C16:1n7/C16:0 ratio was noted (Fig. 2B). Regarding lobular inflammation, the C18:0/C16:0 ratio significantly decreased ($P = 0.04$) and the C16:1n7/C16:0 ratio significantly increased ($P < 0.01$) with an increase in the score (Fig. 2C). Regarding hepatocellular ballooning, the C18:0/C16:0 ratio significantly decreased ($P < 0.01$) and the C16:1n7/C16:0 ratio significantly increased ($P < 0.01$) with an increase in the score (Fig. 2D). Similarly, the C18:0/C16:0 ratio significantly decreased ($P < 0.01$) and the C16:1n7/C16:0 ratio significantly increased ($P < 0.01$) with an increase in the fibrosis score (Fig. 2E).

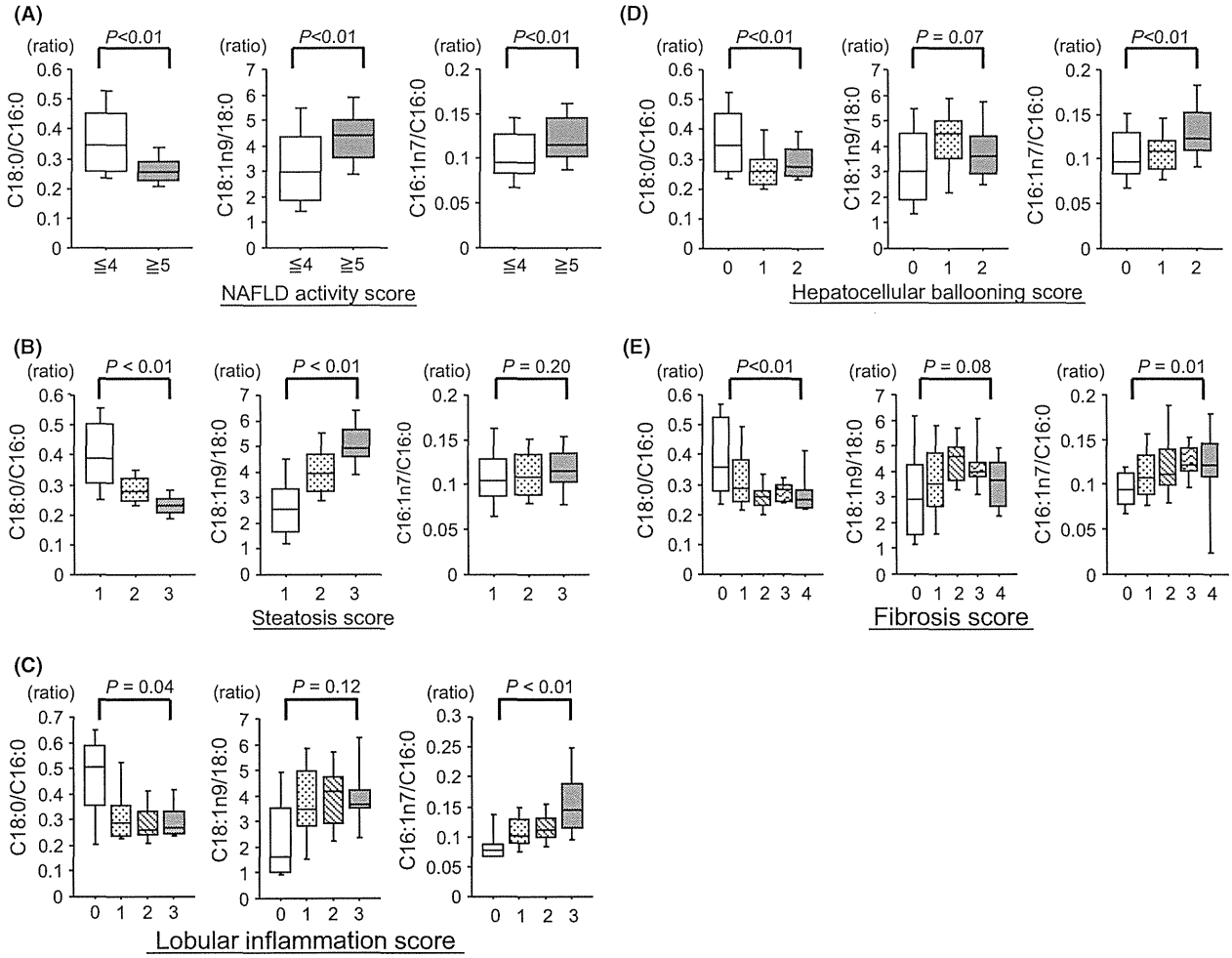

Fig. 2. Relationship between the histopathological findings of the liver and fatty acid composition ratio. The association between the histopathological findings of the liver and fatty acid composition ratio was evaluated using the Spearman's rank correlation coefficient. (A) NAS, (B) steatosis score, (C) lobular inflammation score, (D) hepatocellular ballooning score and (E) fibrosis score.

Expression of fatty acid metabolism-related genes

The gene expression levels of enzymes involved in fatty acid metabolism in liver tissue were investigated. Samples of 65 (SS: 35, NASH: 30) patients were subjected to RTD-PCR, and the gene expression levels of seven enzymes: SCD1, ELOVL6, fatty acid synthase (FAS), sterol regulatory element-binding protein-1c (SREBP-1c), acetyl-CoA carboxylase (ACC), peroxisome proliferator-activated receptor-α (PPARα) and PPARγ were measured. The expression levels of SCD1, ELOVL6, SREBP-1c, FAS and PPARγ were significantly higher in the NASH group than in the SS group, which confirms that the gene expression levels of enzymes involved in fatty acid metabolism were markedly different between the SS and NASH groups (Fig. 3). Thus, the associations between the gene expression levels of these enzymes and histopathological findings (steatosis, inflammation, hepatocellular ballooning and liver fibrosis) were investigated. No significant correlation was noted between the steatosis score and the expression of the fatty acid metabolism-related genes (Fig. 4A); however, a significant correlation was observed between the lobular inflammation score and SCD1 expression ($P < 0.01$), and the gene expression level rose as inflammation progressed in liver tissue (Fig. 4B). The hepatocellular ballooning score was also significantly correlated with the individual gene expression levels of SCD1, ELOVL6, SREBP-1c, FAS, ACC and PPARγ, and expression levels increased as the score rose (Fig. 4C). The fibrosis score was correlated with SREBP-1c expression, but no significant correlation with any other related genes was noted (Fig. 4D).

Finally, we performed a multiple linear regression analysis to calculate age-, sex- and BMI-adjusted coefficients between the histological scores of the liver and experimental parameters such as fatty acid composition, insulin resistance and gene expression (Table 4). In univariate analysis, the steatosis score was significantly correlated with C18:0/C16:0, C18:1n9/C18:0 and QUICKI. In multivariate analysis using these parameters, C18:0/C16:0 was the factor most associated with the steatosis score. In contrast, the inflammation score was significantly correlated with C16:1n7/C16:0, C18:0/C16:0, C18:1n9/C18:0 and SCD1 in univariate analysis and C16:1n7/C16:0 was identified to be the factor most associated with the score in multivariate analysis. The ballooning score was significantly correlated with multiple factors as shown in Table 4 and QUICKI was significantly correlated in multivariate analysis. The fibrosis score was significantly correlated with C18:0/C16:0 only.

Discussion

There have been several reports on fatty acid accumulation in liver tissue in NAFLD. Myristic acid (C14:0), palmitic acid (C16:0) and oleic acid (C18:0) were increased in NAFLD liver tissue in a mouse model (19), and decreases in γ-linolenic acid (C18:3n6) and arachidonic acid (20:4n6) and an increase in the ratios of n-6 and n-3 fatty acids were observed in humans, although the number of cases was small (14). Similar to these findings, the various fatty acid contents of liver tissue were increased in our NAFLD patients. In addition to these fatty acid contents, we closely investigated the fatty acid composition ratios and fatty acid-metabolizing enzymes in the liver tissue in the SS and NASH groups. Regarding the fatty acid composition ratio, significant differences were noted in the C18:0/C16:0, C18:1n9/C18:0 and C16:1n7/C16:0 ratios between the SS and NASH groups, which confirms that the composition ratio of fatty acids is closely associated with the

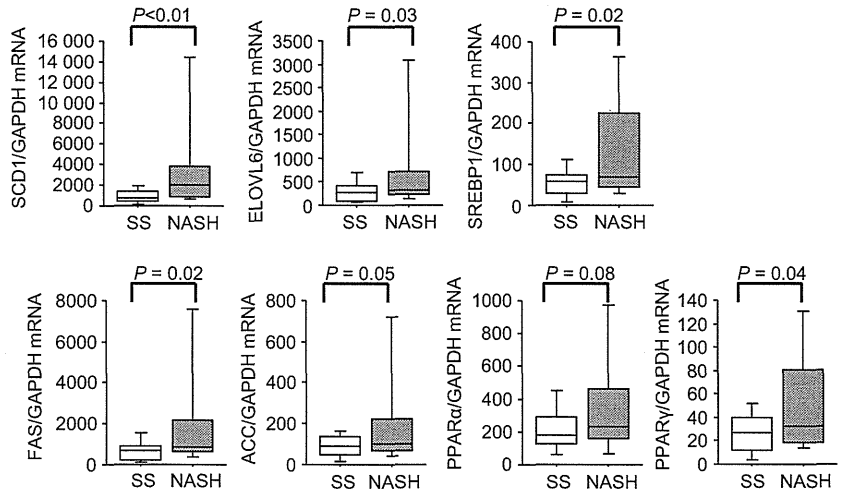

Fig. 3. Expression of fatty acid metabolism-related genes in liver tissue. In 65 patients (SS: 35, NASH: 30), the expression levels of fatty acid metabolism-related genes were measured using RT-PCR, and evaluated using the Mann–Whitney *U*-test.

pathology of NASH, such as the severities of steatosis, inflammation, hepatocellular disorders, and fibrosis. To the best of our knowledge, this is the first report on the association of the liver tissue fatty acid composition ratio with the severities of liver tissue inflammation and hepatocellular disorders in NASH. The fatty acid content of liver tissue was expected to increase in patients with advanced hepatic steatosis; however, significant changes in the fatty acid composition ratios suggested that not all fatty acids homogenously increase. Of the changes in fatty acid composition ratios observed in the SS and NASH groups, a decrease in the C18:0/C16:0 ratio and an increase in the C18:1n9/18:0 ratio (i.e. relative increases in C16:0 and C18:1n9) were associated with steatosis and insulin resistance, and an increase in the C16:1n7/16:0 ratio (i.e. a relative increase in C16:1n7) was associated with liver tissue inflammation and hepatocellular disorders. These results revealed that fatty acid components change depending on pathological differences in liver tissue in NAFLD patients.

There are two main pathways of fatty acid accumulation in the liver. The close involvement of insulin resistance in both pathways has been clarified (20, 21). The hydrolysis of fat tissue occurs in the presence of insulin resistance and increases free fatty acid inflow into the liver in one pathway. In the other, related genes, such as the SREBP-1c gene and downstream SCD1 and FAS genes, are activated in the liver in the presence of high

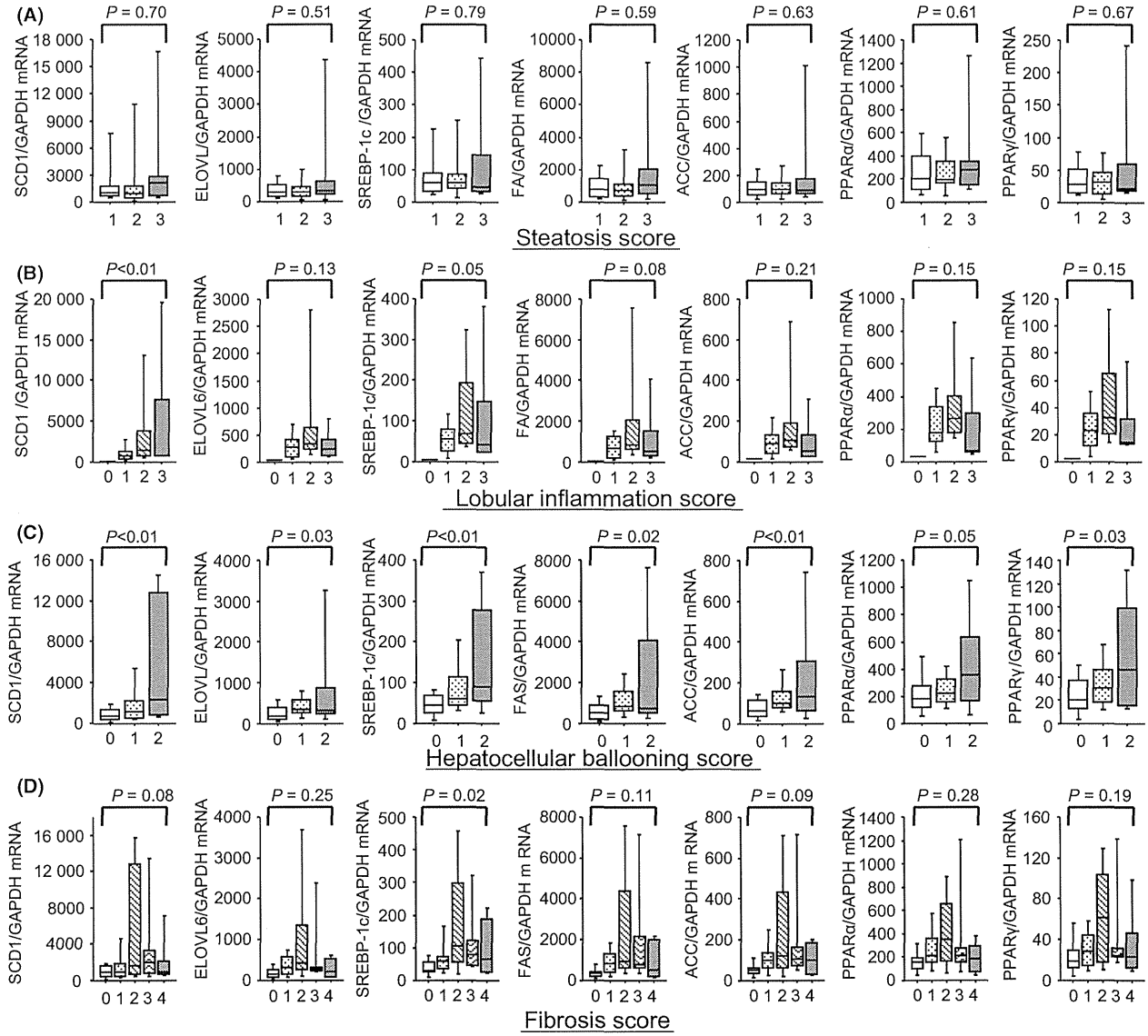

Fig. 4. Relationship between the histopathological findings of the liver and the expression levels of fatty acid metabolism-related genes. The association of the progression of the following items and expression of the fatty acid metabolism-related genes measured in liver tissue using RT-PCR was investigated: (A) steatosis score, (B) lobular inflammation score, (C) hepatocellular ballooning score and (D) fibrosis.

Table 4. Multivariate correlation between histological scores, insulin resistance and genes adjusted for age, gender and BMI

	Steatosis score			Inflammation score			Ballooning score			Fibrosis score		
	Coefficient	UA *P*-value	MA *P*-value	Coefficient	UA *P*-value	MA *P*-value	Coefficient	UA *P*-value	MA *P*-value	Coefficient	UA *P*-value	MA *P*-value
C18:0/C16:0	−0.610	<0.0001	0.0092	−0.315	0.0022	0.4248	−0.310	0.0016	0.3965	−0.289	0.0040	–
C16:1n7/C16:0	0.084	0.4071	–	0.339	0.0010	0.0191	0.255	0.0106	0.2753	0.141	0.1695	–
C18:1n9/C18:0	0.575	<0.0001	0.2387	0.224	0.0302	0.5603	0.243	0.0140	0.5163	0.184	0.0689	–
HOMA-IR	0.070	0.5211	–	0.137	0.2268	–	0.112	0.3083	–	−0.007	0.9485	–
QUICK I	−0.282	0.0108	0.1421	−0.183	0.1180	–	−0.271	0.0163	0.0200	−0.123	0.2901	–
SCD1	0.093	0.4725	–	0.266	0.0386	0.1785	0.321	0.0077	0.2904	0.067	0.5904	–
ELOVL6	0.16	0.1941	–	0.161	0.2177	–	0.283	0.0201	0.8737	0.037	0.7673	–
SREBP-1c	0.104	0.4349	–	0.249	0.0591	–	0.336	0.0064	0.0559	0.118	0.3534	–
FAS	0.148	0.2543	–	0.195	0.1340	–	0.320	0.0083	0.3309	0.085	0.4949	–
ACC	0.142	0.2902	–	0.159	0.2380	–	0.254	0.0441	0.1917	0.040	0.7539	–
PPARα	0.131	0.3222	–	0.170	0.2005	–	0.232	0.0637	–	0.028	0.8227	–
PPARγ	0.136	0.3243	–	0.155	0.2631	–	0.215	0.1003	–	0.030	0.8195	–

MA, multivariate analysis; PPARα, peroxisome proliferator-activated receptor-α; UA, univariate analysis.

blood insulin and glucose levels (22) and promote glucose uptake in the liver, enhancing the *de novo* synthesis of C16:0 through acetyl-CoA.

C16:0 is considered to be a toxic fatty acid for liver tissue. TGs in the liver and microsomal saturated fatty acids increased in mice fed a saturated fatty acid-enriched diet, and elevations in the activity of liver caspase-3 and transaminase levels were confirmed (23). Saturated fatty acids, such as C16:0, are not readily esterified and exhibit strong cytotoxicity in the liver (24). It is assumed that toxicity is avoided by the conversion of these saturated fatty acids to unsaturated fatty acids, such as C16:1n7 and C18:1n9, through elongation by ELOVL6 and desaturation by SCD1. As both ELOVL6 and SCD1 were controlled by SREBP-1c, their expressions are related to each other.

It has been previously reported that the expression of these genes was associated with the pathology of NASH in an animal model (25). Matsuzaka et al. have also shown that the expression level of ELOVL6 in the liver was correlated with the inflammation of liver tissue in a mouse model with NASH and was also increased in NASH patients (26). These results are consistent with our results. In this study, we evaluated the relationship between fatty acid metabolism and NASH pathology by the simultaneous examination of the fatty acid composition ratio around C16:0, fatty acid metabolic gene expression and histopathology of the liver in the same liver samples of many patients. The analysis of age-, sex- and BMI-adjusted associations between the histological scores of the liver and experimental parameters showed that a decrease in the C18:0/C16:0 ratio, an increase in the C16:1n7/16:0 ratio, and an increase in the expression of fatty acid metabolism-related genes including SCD1 and ELOVL6 correlated with inflammation or ballooning of liver tissue. Taking our results together with previous reports, fatty acid metabolism in the liver according to the development of NASH can be explained as follows.

First, a decrease in the C18:0/C16:0 ratio is because of an increase in C16:0 without an increase in the fatty acid metabolism-related genes. Next, an increase in the expression of the fatty acid metabolism-related genes including SCD1 and ELOVL6 occurs and correlates with inflammation and the ballooning of hepatocytes in liver tissue. Finally, it becomes difficult to sufficiently convert C16:0 to C18:0 by ELOVL6, and a compensatory increase in the conversion of C16:0 to C16:1n7 controlled by SCD1 occurs. Consequently, the increase in C16:1n7/C16:0 correlates with inflammation in liver tissue with the highest correlation coefficient. Therefore, our results suggest that the acceleration of overall hepatic fatty acid metabolism is more important for the pathogenesis of NASH than the expression levels of ELOVL6 in patients with NASH.

In conclusion, analysis of the liver tissue fatty acid composition and gene expression showed that an enhancement of the fatty acid metabolic pathway centring on C16:0 contributed to the progression of SS to NASH. Elucidating these changes in the metabolic pathway may lead to the development of a drug that could prevent the progression to NASH.

Acknowledgements

The authors thank Maki Kawamura, Nami Nishiyama and Mikiko Nakamura for technical assistance.

Financial support: This work was supported in part by research grants from the Ministry of Education, Culture, Sports, Science and Technology of Japan.

Conflict of interest: The authors do not have any disclosures to report.

References

1. Ogden CL, Carroll MD, Curtin LR, *et al.* Prevalence of overweight and obesity in the United States, 1999-2004. *JAMA* 2006; **295**: 1549–55.
2. Kojima S, Watanabe N, Numata M, Ogawa T, Matsuzaki S. Increase in the prevalence of fatty liver in Japan over the past 12 years: analysis of clinical background. *J Gastroenterol* 2003; **38**: 954–61.
3. Browning JD, Horton JD. Molecular mediators of hepatic steatosis and liver injury. *J Clin Invest* 2004; **114**: 147–52.
4. Diehl AM, Li ZP, Lin HZ, Yang SQ. Cytokines and the pathogenesis of non-alcoholic steatohepatitis. *Gut* 2005; **54**: 303–6.
5. Angulo P, Keach JC, Batts KP, Lindor KD. Independent predictors of liver fibrosis in patients with nonalcoholic steatohepatitis. *Hepatology* 1999; **30**: 1356–62.
6. Sanyal AJ, Unalp A; Investigators NC. Pioglitazone, vitamin E, or placebo for nonalcoholic steatohepatitis REPLY. *N Engl J Med* 2010; **363**: 1186–86.
7. Zein CO, Yerian LM, Gogate P, *et al.* Pentoxifylline improves nonalcoholic steatohepatitis: a randomized placebo-controlled trial. *Hepatology* 2011; **54**: 1610–9.
8. Nozaki Y, Fujita K, Yoneda M, *et al.* Long-term combination therapy of ezetimibe and acarbose for non-alcoholic fatty liver disease. *J Hepatol* 2009; **51**: 548–56.
9. Sanyal AJ, Campbell-Sargent C, Mirshahi F, *et al.* Nonalcoholic steatohepatitis: association of insulin resistance and mitochondrial abnormalities. *Gastroenterology* 2001; **120**: 1183–92.
10. Chitturi S, Abeygunasekera S, Farrell GC, *et al.* NASH and insulin resistance: insulin hypersecretion and specific association with the insulin resistance syndrome. *Hepatology* 2002; **35**: 373–9.
11. Pascale A, Pais R, Ratziu V. An overview of nonalcoholic steatohepatitis: past, present and future directions. *J Gastrointest Liver Dis* 2010; **19**: 415–23.
12. Matsuzaka T, Shimano H, Yahagi N, *et al.* Crucial role of a long-chain fatty acid elongase, Elovl6, in obesity-induced insulin resistance. *Nat Med* 2007; **13**: 1193–202.
13. Li ZZ, Berk M, Mcintyre TM, Feldstein AE. Hepatic lipid partitioning and liver damage in nonalcoholic fatty liver disease: role of stearoyl-CoA desaturase. *J Biol Chem* 2009; **284**: 5637–44.
14. Puri P, Baillie RA, Wiest MM, *et al.* A lipidomic analysis of nonalcoholic fatty liver disease. *Hepatology* 2007; **46**: 1081–90.
15. Matteoni CA, Younossi ZM, Gramlich T, *et al.* Nonalcoholic fatty liver disease: a spectrum of clinical and pathological severity. *Gastroenterology* 1999; **116**: 1413–9.
16. Kleiner DE, Brunt EM, Van Natta M, *et al.* Design and validation of a histological scoring system for nonalcoholic fatty liver disease. *Hepatology* 2005; **41**: 1313–21.
17. Defronzo RA, Tobin JD, Andres R. Glucose clamp technique: a method for quantifying insulin secretion and resistance. *Am J Physiol* 1979; **237**: E214–23.
18. Honda M, Yamashita T, Ueda T, *et al.* Different signaling pathways in the livers of patients with chronic hepatitis B or chronic hepatitis C. *Hepatology* 2006; **44**: 1122–38.
19. Wang X, Cao YZ, Fu YW, Guo GF, Zhang XY. Liver fatty acid composition in mice with or without nonalcoholic fatty liver disease. *Lipids Health Dis* 2011; **10**: 234.
20. Donnelly KL, Smith CI, Schwarzenberg SJ, *et al.* Sources of fatty acids stored in liver and secreted via lipoproteins in patients with nonalcoholic fatty liver disease. *J Clin Invest* 2005; **115**: 1343–51.
21. Fabbrini E, Sullivan S, Klein S. Obesity and nonalcoholic fatty liver disease: biochemical, metabolic, and clinical implications. *Hepatology* 2010; **51**: 679–89.
22. Shimomura L, Bashmakov Y, Ikemoto S, *et al.* Insulin selectively increases SREBP-1c mRNA in the livers of rats with streptozotocin-induced diabetes. *Proc Natl Acad Sci USA* 1999; **96**: 13656–61.
23. Wang D, Wei YR, Pagliassotti MJ. Saturated fatty acids promote endoplasmic reticulum stress and liver injury in rats with hepatic steatosis. *Endocrinology* 2006; **147**: 943–51.
24. Listenberger LL, Han XL, Lewis SE, *et al.* Triglyceride accumulation protects against fatty acid-induced lipotoxicity. *Proc Natl Acad Sci USA* 2003; **100**: 3077–82.
25. Miyazaki M, Flowers MT, Sampath H, *et al.* Hepatic stearoyl-CoA desaturase-1 deficiency protects mice from carbohydrate-induced adiposity and hepatic steatosis. *Cell Metab* 2007; **6**: 484–96.
26. Matsuzaka T, Atsumi A, Matsumori R, *et al.* Elovl6 promotes nonalcoholic steatohepatitis. *Hepatology* 2012; **56**: 2199–208.

Supporting information

Additional Supporting Information may be found in the online version of this article:

Table S1. Differences of fatty acid composition rates in liver tissue among male, premenopausal female, postmenopausal female.

HEPATOLOGY
Official Journal of the American Association for the Study of Liver Diseases

Gd-EOB-DTPA-Enhanced Magnetic Resonance Imaging and Alpha-Fetoprotein Predict Prognosis of Early-Stage Hepatocellular Carcinoma

Taro Yamashita,[1,2] Azusa Kitao,[3] Osamu Matsui,[3] Takehiro Hayashi,[2] Kouki Nio,[2] Mitsumasa Kondo,[2] Naoki Ohno,[4] Tosiaki Miyati,[4] Hikari Okada,[2] Tatsuya Yamashita,[2] Eishiro Mizukoshi,[2] Masao Honda,[2] Yasuni Nakanuma,[5] Hiroyuki Takamura,[6] Tetsuo Ohta,[6] Yasunari Nakamoto,[7] Masakazu Yamamoto,[8] Tadatoshi Takayama,[9] Shigeki Arii,[10] XinWei Wang,[11] and Shuichi Kaneko[2]

The survival of patients with hepatocellular carcinoma (HCC) is often individually different even after surgery for early-stage tumors. Gadolinium ethoxybenzyl diethylenetriamine pentaacetic acid (Gd-EOB-DTPA)-enhanced magnetic resonance imaging (MRI) has been introduced recently to evaluate hepatic lesions with regard to vascularity and the activity of the organic anion transporter OATP1B3. Here we report that Gd-EOB-DTPA-enhanced MRI (EOB-MRI) in combination with serum alpha-fetoprotein (AFP) status reflects the stem/maturational status of HCC with distinct biology and prognostic information. Gd-EOB-DTPA uptake in the hepatobiliary phase was observed in ~15% of HCCs. This uptake correlated with low serum AFP levels, maintenance of hepatocyte function with the upregulation of *OATP1B3* and *HNF4A* expression, and good prognosis. By contrast, HCC showing reduced Gd-EOB-DTPA uptake with high serum AFP levels was associated with poor prognosis and the activation of the oncogene *FOXM1*. Knockdown of *HNF4A* in HCC cells showing Gd-EOB-DTPA uptake resulted in the increased expression of *AFP* and *FOXM1* and the loss of *OATP1B3* expression accompanied by morphological changes, enhanced tumorigenesis, and loss of Gd-EOB-DTPA uptake *in vivo*. HCC classification based on EOB-MRI and serum AFP levels predicted overall survival in a single-institution cohort (n = 70), and its prognostic utility was validated independently in a multi-institution cohort of early-stage HCCs (n = 109). *Conclusion*: This noninvasive classification system is molecularly based on the stem/maturation status of HCCs and can be incorporated into current staging practices to improve management algorithms, especially in the early stage of disease. (HEPATOLOGY 2014;60:1674-1685)

Liver cancer is the fifth most commonly diagnosed cancer and the second most frequent cause of cancer death in men worldwide.[1] Among primary liver cancers, hepatocellular carcinoma (HCC) represents the major histological subtype, accounting for 70-86% of cases of primary liver cancer.[1] Several staging systems are currently available for HCC classification and include Tumor Node

Abbreviations: AFP, alpha-fetoprotein; BCLC, Barcelona Clinic Liver Cancer; EOB-MRI, gadolinium ethoxybenzyl diethylenetriamine pentaacetic acid-enhanced magnetic resonance imaging; FOXM1, forkhead box protein M1; Gd-EOB-DTPA, gadolinium ethoxybenzyl diethylenetriamine pentaacetic acid; HCC, hepatocellular carcinoma; HNF4α, hepatocyte nuclear factor 4 alpha; IHC, immunohistochemistry; MRI, magnetic resonance imaging; NOD/SCID, nonobese diabetic, severe combined immunodeficient; OATPs, organic anion transporting polypeptides; qRT-PCR, quantitative reverse-transcription polymerase chain reaction; SI, signal intensity; TNM, tumor node metastasis.

From the [1]Department of General Medicine, Kanazawa University Graduate School of Medical Science, Kanazawa, Ishikawa, Japan; [2]Department of Gastroenterology, Kanazawa University Graduate School of Medical Science, Kanazawa, Ishikawa, Japan; [3]Department of Radiology, Kanazawa University Graduate School of Medical Science, Kanazawa, Ishikawa, Japan; [4]Faculty of Health Sciences, Institute of Medical, Pharmaceutical and Health Sciences, Kanazawa University, Kanazawa, Ishikawa, Japan; [5]Department of Pathology, Kanazawa University Graduate School of Medical Science, Kanazawa, Ishikawa, Japan; [6]Department of Gastroenterologic Surgery, Kanazawa University Graduate School of Medical Science, Kanazawa, Ishikawa, Japan; [7]Second Department of Internal Medicine, Fukui University School of Medicine, Fukui, Japan; [8]Department of Surgery, Institute of Gastroenterology, Tokyo Women's Medical University, Tokyo, Japan; [9]Department of Digestive Surgery, Nihon University School of Medicine, Tokyo, Japan; [10]Department of Hepato-Biliary-Pancreatic Surgery, Tokyo Medical and Dental University, Tokyo, Japan; [11]Laboratory of Human Carcinogenesis, Center for Cancer Research, National Cancer Institute, Bethesda, MD, USA.

Received September 19, 2013; accepted February 20, 2014.

Metastasis (TNM) and Barcelona Clinic Liver Cancer (BCLC) staging, which are based on tumor number and size, vascular invasion, metastatic status, hepatic reserve, and performance status.[2] These systems can provide an approximate estimate of patients' survival, but patients diagnosed at the same disease stage sometimes show a different prognosis. This is most likely because these systems do not include an assessment of the malignant phenotype of the tumor, which would be especially important in those patients diagnosed at the early stage of disease. To overcome these limitations, gene expression profiling technologies have been applied to classify HCC. In particular, the stemness of HCC is currently of great interest because its gene expression profile reflects the malignant nature of the tumor.[3-7] However, the application of these new technologies still needs to be validated externally prior to their implementation in clinical practice.

The hallmark of HCC diagnosis has been image analysis based on vascularity. Gadolinium ethoxybenzyl diethylenetriamine pentaacetic acid (Gd-EOB-DTPA) is a liver-specific magnetic resonance imaging (MRI) contrast agent introduced specifically to improve the detection of liver lesions.[8] Gd-EOB-DTPA-enhanced MRI (EOB-MRI) has been used to evaluate liver tumors in Europe since 2004, in the USA and Japan since 2008, and in China since 2010. Gd-EOB-DTPA is characterized by its rapid and specific uptake by hepatocytes by way of organic anion transporting polypeptides (OATPs) expressed in the sinusoidal membrane. Therefore, Gd-EOB-DTPA uptake in the liver is considered to reflect hepatocyte function.[9] Among OATP1A2, 1B1, 1B3, and 2B1, only OATP1B3 expression was found to correlate with the enhancement ratio on EOB-MRI, indicating that it transports Gd-EOB-DTPA into HCC cells.[10] It is generally accepted that ~85% of HCCs show hypointensity in the hepatobiliary phase of EOB-MRI compared to the noncancerous background liver, with a reduction of OATP1B3 protein or *OATP1B3* gene expression in the tumor.[10,11] However, atypical Gd-EOB-DTPA uptake in the hepatobiliary phase is observed in the remaining 15% of HCCs, and the molecular phenotype and clinical features of these HCCs remain to be elucidated.

We hypothesized that EOB-MRI findings may vary in different tumor subtypes with distinct biology. Therefore, in this study we evaluated the molecular profiles of HCCs in a single-institute cohort determined from the EOB-MRI findings using quantitative reverse-transcription polymerase chain reaction (qRT-PCR), microarray, and immunohistochemistry (IHC) analyses. To clarify the clinical utility of the EOB-MRI findings, we also evaluated the prognosis of a multicenter cohort of patients with early-stage HCC who underwent radical resection.

Materials and Methods

Patients. A total of 417 patients who received surgical resection for HCC were enrolled in this study. Seventy patients underwent EOB-MRI for the diagnosis of HCC and received surgical resection at Kanazawa University Hospital from 2008 to 2011. Survival analysis was performed in this single-institute cohort (Cohort 1) and prognosis was evaluated every 6 months. The final evaluation of survival was performed in October 2011. From these 70 patients, 62 tumor and nontumor samples were snap-frozen in liquid nitrogen and used for qRT-PCR.

For microarray analysis, we assessed 238 patients who received surgical resection of HCC at the Liver Cancer Institute of Fudan University. EOB-MRI was not performed in these patients because Gd-EOB-DTPA had not yet been introduced in China. Their clinicopathologic characteristics and prognostic data have been described previously.[12]

To evaluate the survival of early-stage HCCs, we enrolled 109 patients who received EOB-MRI and surgical resection at Tokyo Medical and Dental University Hospital, Tokyo Women's Medical University Hospital, Nihon University School of Medicine Itabashi Hospital, Niigata University Medical & Dental Hospital, Hyogo College of Medicine Hospital, or Kurume

Supported by Health and Labor Sciences Research Grants for "Development of novel molecular markers and imaging modalities for earlier diagnosis of hepatocellular carcinoma," Grants from the Ministry of Education, Culture, Sports, Science, and Technology of Japan, the National Cancer Center Research and Development Fund (23-B-5), and the Intramural Research Program Grant (Z01 BC 010313) of the Center for Cancer Research, US National Cancer Institute.

Address reprint requests to: Taro Yamashita, M.D., Ph.D., Assistant Professor, Department of Gastroenterology/General Medicine, Kanazawa University Graduate School of Medical Science, 13-1 Takara-Machi, Kanazawa, Ishikawa 920-8641, Japan. E-mail: taroy@m-kanazawa.jp; fax: +81-76-234-4250.

View this article online at wileyonlinelibrary.com.
DOI 10.1002/hep.27093
Potential conflict of interest: Dr. Matsui is on the speakers' bureau for Bayer.

University Hospital from 2008 to 2009 (Cohort 2). The prognosis of these patients was evaluated every year, and the final evaluation of survival was performed in February 2012.

This study was approved by the Institutional Review Board at each study center and all patients provided written informed consent.

EOB-MRI. EOB-MRI was performed before surgical resection using a 1.5 or 3.0 Tesla MRI system with a fat-suppressed 2D or 3D gradient echo T1-weighted sequence (relaxation time / echo time [TR/TE] = 3.2-3.6/1.6-2.3 ms, flip angle 10-15°, field of view 33-42 cm, matrix 128-192 × 256-512, slice thickness 4.0-8.0 mm). A dose of 0.025 mmol/kg Gd-EOB-DTPA (Primovist; Bayer Schering Pharma, Berlin, Germany) was injected intravenously and the hepatobiliary phase was obtained at 15-20 minutes after the injection.

All abdominal MRI data of the HCC patients were generated at Kanazawa University Hospital and image analysis was performed retrospectively by two radiologists (A.K. and O.M.) without knowledge of the clinical and pathological results. The signal intensity (SI) of the tumor was measured within the region of interest, which was determined as the maximum oval area at the largest section of the tumor. The SI of the adjacent background liver was also measured within a region of interest of the same size, while avoiding large vessels. The nodules were classified into the two following types: hypointense HCC, which was defined as showing a lower SI than that of the surrounding liver (tumor SI / background SI <1.0) in the hepatobiliary phase, and hyperintense HCC, which was defined as showing an equal or higher SI (tumor SI / background SI ≥ 1.0).

For the mouse study, EOB-MRI was performed using a 0.4 T MRI system with a fat-suppressed 3D gradient echo T1-weighted sequence (TR/TE = 66.5/4.0 ms, flip angle 40°, field of view 10 cm, matrix 224 × 192, slice thickness 1.0 mm). A dose of 0.025 mmol/kg Gd-EOB-DTPA (Bayer Schering Pharma) was injected through the tail vein, and the hepatobiliary phase was obtained at 12-20 minutes after the injection.

Xenotransplantation of Primary HCC in Immunodeficient Mice and* HNF4A *Knockdown. Primary HCC tissue was dissected and digested in 1 mg/mL type 4 collagenase solution (Sigma-Aldrich Japan, Tokyo, Japan) at 37°C for 15-30 minutes. Contaminated red blood cells were lysed with an ammonium chloride solution (STEMCELL Technologies, Vancouver, BC, Canada) on ice for 5 minutes. $CD45^+$ leukocytes and annexin V^+ apoptotic cells were removed by an autoMACS-pro cell separator and magnetic beads (Miltenyi Biotec, Tokyo, Japan). The cells were suspended 1:1 in 200 μL Dulbecco's modified Eagle's medium (DMEM) and Matrigel (BD Biosciences) and injected subcutaneously into 6-week-old NOD/SCID mice (NOD/NCrCRl-*Prkdc*^{scid}) purchased from Charles River Laboratories (Wilmington, MA). EOB-MRI was performed to evaluate Gd-EOB-DTPA uptake in the subcutaneous tumor at the hepatobiliary phase, and the subcutaneous tumor was dissected and digested as described above, and subsequently cultured in DMEM. *HNF4A* knockdown was performed using pGFP-V-RS vectors (OriGene Technologies, Rockville, MD), allowing stable delivery of the short hairpin RNA (shRNA) expression cassette against *HNF4A* or scramble sequence into host cells by way of a replication-deficient retrovirus. Infected HCC cells were grown in DMEM containing 1 μg/mL puromycin (Sigma-Aldrich Japan) for 7 days to establish stable shRNA-expressing HCC cells. Western blotting and immunofluorescence analyses were performed using an antihuman HNF4α C11F12 antibody (Cell Signaling Technology, Danvers, MA) and a mouse monoclonal antihuman OATP1B3 MDQ/5F260 antibody (Novus Biologicals, Littleton, CO), essentially as described previously.[13] Control or Sh-HNF4A-transfected HCC cells were injected subcutaneously into NOD/SCID mice, and tumor volume and survival were evaluated every 2-3 days. The protocol was approved by the Kanazawa University Animal Care and Use Committee and the Kanazawa University Genetic Modification Experiment Committee.

Microarray Analysis. The 238 HCC cases from the Liver Cancer Institute of Fudan University with available microarray data and clinicopathologic and prognostic data have been described previously.[12] BRB-ArrayTools software (v. 3.8.1) was used for class comparison analysis. Hierarchical clustering analysis was performed with Genesis software (v. 1.6.0 beta). Canonical pathway and transcription factor analyses were performed using MetaCore software (http://www.genego.com). Interaction network analysis was performed using Ingenuity Pathway Analysis software (http://www.ingenuity.com).

qRT-PCR Analysis. Total RNA was extracted using an RNeasy Mini Kit (Qiagen, Valencia, CA) according to the manufacturer's instructions. The expression of selected genes was determined in triplicate using the Applied Biosystems 7900HT Sequence Detection System (Applied Biosystems, Foster City, CA) and the $-\Delta\Delta CT$ method. The following probes were used: *AFP*, Hs00173490_m1; *FOXM1*, Hs01073586_m1; *OATP1B3*, Hs00251986_m1; *CYP3A4*, Hs00430021_m1; and *18S*, Hs99999901_s1 (Applied Biosystems).

IHC Analysis. IHC was performed using Envision+ kits (Dako Japan, Tokyo, Japan) as described previously.[14] Mouse monoclonal antihuman Ki-67 antigen MIB-1 (Dako Japan), mouse monoclonal antihuman OATP1B3 MDQ/5F260 (Novus Biologicals), rabbit monoclonal antihuman HNF4α C11F12 (Cell Signaling Technology), mouse monoclonal antihuman FOXM1 0.T.181 (Abcam, Cambridge, MA), mouse monoclonal antihuman glypican-3 1G12 (BioMosaics, Burlington, VT), and mouse monoclonal antiglutamine synthetase clone GS-6 (Millipore, Billerica, MA) antibodies were used. The staining area and intensities were evaluated in each sample and graded from 0-3 (0, 0-5%; 1, 5-25%; 2, 25-50%; 3, >50%) and 0-2 (0, negative; 1, weak; 2, strong), respectively. The sum of the area and intensity scores of each marker (IHC score) were calculated. Samples were defined as marker-high (IHC score $\geq$3) or -low (IHC score $\leq$2). The Ki-67 labeling index was calculated as described previously.[14]

Statistical Analysis. Mann-Whitney, χ^2, Fisher's exact, and Kruskal-Wallis tests were used to compare the clinicopathologic characteristics and gene expression data. The correlation of the gene expression data was evaluated by Spearman's rank correlation coefficient. Kaplan-Meier survival analysis with the log-rank test was performed to compare patient survival. All analyses were performed using GraphPad Prism software v. 5.0.1 (GraphPad Software, San Diego, CA).

Results

EOB-MRI Findings and Molecular Characteristics of HCC. Nine of the 70 HCC cases (12.9%) in Cohort 1 were diagnosed with hyperintense HCC on EOB-MRI (Fig. 1A). Analysis of the clinicopathologic characteristics of hyper- or hypointense HCCs revealed that hyperintense HCCs were significantly associated with low serum alpha-fetoprotein (AFP) levels (Table 1). There was no significant difference between hyper- and hypointense HCCs in terms of other factors, including tumor size, number, TNM and BCLC stages, surgical procedures, and elapsed time between MRI and surgery. We confirmed the overexpression of OATP1B3, a transporter responsible for the uptake of Gd-EOB-DTPA in hepatocytes, in hyperintense HCCs by qRT-PCR and IHC (Fig. 1B).

To understand the transcriptomic characteristics of HCCs overexpressing *OATP1B3*, we analyzed the microarray data of an additional 238 HCC cases.[12] *OATP1B3*-high and -low HCCs were defined as HCCs with a T/N ratio $\geq$1.0 and <1.0, respectively, as used for the evaluation of hyperintense HCCs (tumor SI / background SI $\geq$1.0). The frequency of *OATP1B3*-high HCCs was 15.1% (36 of the 238 HCC cases), almost comparable to the frequency of hyperintense HCCs reported thus far. Class-comparison analysis yielded a total of 974 genes that were differentially expressed between *OATP1B3*-high and -low HCCs ($P < 0.001$). Hierarchical cluster analysis of this 974 gene set (*OATP1B3* gene signature) separated HCCs into two branches (B1 and B2) (Fig. 1C). Thirty-four of the 36 *OATP1B3*-high HCCs (blue box) were classified in the left branch (B1), while *OATP1B3*-low HCCs were clustered in both branches. The prognosis of HCC patients clustered in B1 was significantly better than those clustered in B2 ($P = 0.02$) (Supporting Fig. S1). Genes associated with mature hepatocyte function such as *ALB* and *CYP3A4* were significantly up-regulated in the HCCs clustered in B1, and the known hepatic stem/progenitor markers *KRT19* and *EPCAM*, as well as the G1/S cell cycle marker *MKI67*, were significantly up-regulated in the HCCs clustered in B2 (Fig. 1D).

Pathway analysis indicated that *OATP1B3*-high HCCs showed maintenance of mature hepatocyte function and decreased cell proliferation and Wnt signaling (Fig. 1E), which are known to be activated during liver development and regeneration.[15] Transcription factor analysis identified eight genes (*HNF4A, NFIA, NR3C1, NR1I3, ESR1, NR1H3, MLXIPL*, and *NFE2L2*) as candidate transcription factors that were significantly activated in *OATP1B3*-high HCCs ($P < 0.005$) (Fig. 1F). These transcription factors are known to play a pivotal role in liver development and in the regulation of hepatocyte functions including lipid, bile, carbohydrate, and xenobiotic metabolism.[16] By contrast, only one gene (*FOXM1*) was identified as a candidate transcription factor activated in *OATP1B3*-low HCCs. The forkhead box M1 (FOXM1) transcription factor is known to be activated during liver regeneration and regulation of the cell cycle.[17] We investigated the expression of the two transcription factors most strongly activated (*HNF4A* encoding hepatocyte nuclear factor 4 alpha [HNF4α]) or inactivated (*FOXM1*) in hyperintense HCCs (Fig. S2) and validated the results using microarray analyses (Fig. 2A,B).

Although the microarray data revealed distinct molecular portraits associated with liver development and the maturation programs present in hyper- and hypointense HCCs, hierarchical cluster analysis further indicated that a subset of hypointense HCCs (corresponding to the *OATP1B3*-low HCCs clustered in B1)

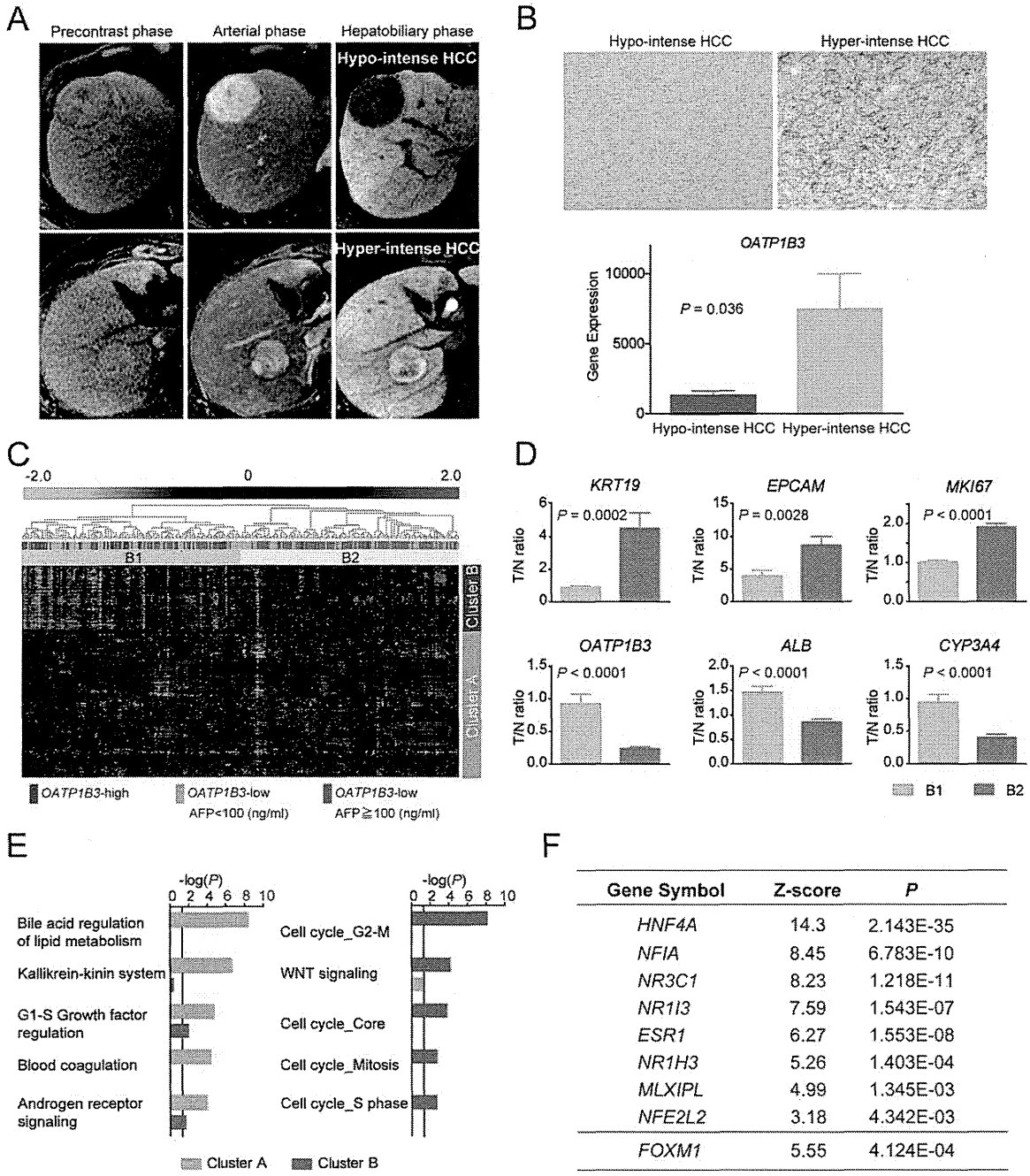

F

Gene Symbol	Z-score	P
HNF4A	14.3	2.143E-35
NFIA	8.45	6.783E-10
NR3C1	8.23	1.218E-11
NR1I3	7.59	1.543E-07
ESR1	6.27	1.553E-08
NR1H3	5.26	1.403E-04
MLXIPL	4.99	1.345E-03
NFE2L2	3.18	4.342E-03
FOXM1	5.55	4.124E-04

Fig. 1. Molecular profiles of HCCs corresponding to the EOB-MRI findings. (A) Representative MRI scans of hypo- and hyperintense HCCs in the precontrast, arterial, and hepatobiliary phases. The T/N signal intensity ratios of the images in the hepatobiliary phase were 0.47 (upper panel) and 1.07 (lower panel). (B) Upper panel: Representative photomicrographs of IHC staining with an anti-OATP1B3 antibody in hypo- and hyperintense HCCs. Lower panel: *OATP1B3* expression in hypo- and hyperintense HCCs. (C) The expression patterns of *OATP1B3* signatures in *OATP1B3*-high (blue box), *OATP1B3*-low AFP-low (<100 ng/mL) (orange box), and *OATP1B3*-low AFP-high (≥100 ng/mL; red box) after hierarchical clustering of genes and samples, shown as a heat map image. Red indicates a high expression level; green indicates a low expression level. *OATP1B3*-high HCCs and *OATP1B3*-low AFP-high HCCs were clustered in B1 (green bar) and B2 (yellow bar), respectively. (D) Representative expression of genes in clusters A (*KRT19, EPCAM*, and *MKI67*) and B (*OATP1B3, ALB*, and *CYP3A4*). The green and orange bars indicate HCCs clustered in B1 and B2, respectively. (E) The activated pathways are identified in clusters A (orange bar) and B (blue bar). (F) Genes encoding transcription factors activated or inactivated in *OATP1B3*-high HCCs.

might show similar gene expression profiles to those observed in hyperintense HCCs. Since serum AFP levels are reportedly related to the stem/maturation subtypes of HCCs with different gene expression profiles,[12] we analyzed the characteristics of *OATP1B3*-low HCCs in 238 cases according to serum AFP levels. Interestingly, *OATP1B3*-low HCCs assigned to the left branch (B1) had low serum AFP

Table 1. Characteristics of HCCs Classified by EOB-MRI in Cohorts 1 and 2

Characteristics	Cohort 1			Cohort 2		
	Hyperintense (n = 9)	Hypointense (n = 61)	P*	Hyperintense (n = 9)	Hypointense (n = 100)	P*
Age (years, mean ± SE)	66.2 ± 3.6	64.6 ± 1.2	0.21	67.2 ± 2.0	66.2 ± 1.0	1.0
Sex (male/female)	7/2	44/17	0.72	9/0	79/21	0.13
Etiology (HBV/HCV/other)	2/3/4	14/23/24	0.95	1/6/0/2	22/56/2/20	0.52
Liver cirrhosis (yes/no)	5/4	33/28	0.94	2/7	42/58	0.25
AFP (ng/mL, mean ± SE)	12.4 ± 1.9	2,157 ± 866	0.03	7.0 ± 2.2	188.4 ± 74	0.03
Histologic grade†						
I-II	1	12		2	16	
II-III	8	38		7	74	
III-IV	0	11	0.25	0	10	0.57
Tumor size (cm, mean ± SE)	4.0 ± 0.9	4.4 ± 0.4	0.79	3.3 ± 0.4	2.6 ± 0.1	0.09
Tumor number (single/multiple)	7/2	48/13	0.95	8/1	86/14	0.81
Macroscopic portal vein invasion (yes/no)	1/8	5/56	0.58	0/9	0/100	
Microscopic portal vein invasion (yes/no)	2/7	27/34	0.21	0/9	11/89	0.59
Tumor-node-metastasis classification (I/II/III)	6/2/1	29/28/4	0.40	7/2/0	75/25/0	0.85
BCLC stage (0/A/B/C)	0/7/1/1	4/30/22/5	0.34	0/9/0/0	27/73/0/0	0.07
Elapsed time between MRI and surgery (days, mean ± SE)	47.0 ± 8.4	51.5 ± 3.2	0.73	17.3 ± 5.0	20.6 ± 3.0	0.50
Surgical procedure (partial resection or segmentectomy/ lobectomy or extended lobectomy)	6/3	35/26	0.60	8/1	86/14	1.0

*Mann-Whitney test, Fisher's exact test, or χ^2 test.
†Edmondson-Steiner.

levels (<100 ng/mL: orange box, Fig. 1C), while the majority of AFP-high (≥100 ng/mL) HCCs (red box, Fig. 1C) were clustered in the right branch (B2). Consistently, the *OATP1B3* gene signature significantly predicted the serum AFP status of 238 HCCs ($P < 0.05$) (Tables S1-3).

OATP1B3 and AFP Expression in HCC Subtypes Related to Stem/Maturational Status. Molecular profiling of tissue samples may be useful for predicting the survival of HCC patients, as reported previously.[18,19] However, such an approach should be established before being applied routinely in a clinical setting. The above data prompted us to hypothesize that EOB-MRI findings and serum AFP levels, in place of molecular profiling techniques, have the potential to categorize HCCs (EOB-AFP classification), thus serving as predictors of survival. We categorized HCCs into three groups (class A: hyperintense HCC, class B: hypointense and AFP-low [<100 ng/mL] HCC, and class C: hypointense and AFP-high [≥100 ng/mL] HCC). The clinicopathologic characteristics of patients with class A, B, and C HCCs in Cohort 1 are shown in Table S4.

We investigated the expression of HNF4α and FOXM1 as well as the G1/S marker Ki-67 by IHC according to the EOB-AFP classification system in Cohort 1 (Fig. 2C). HNF4α was most abundantly expressed in class A HCCs, but its expression was decreased in class B and C HCCs. By contrast, the expression of FOXM1 and Ki-67 was highest in class C HCCs, significantly decreased in class B HCCs, and not detected in class A HCCs. The mean Ki-67 labeling indices in class A, B, and C HCCs were 2.8%, 9.4%, and 18.2%, respectively ($P < 0.0001$) (Fig. 2D). The differences in FOXM1 and HNF4α expression among class A, B, and C HCCs were statistically significant (Fig. 2E).

We further investigated the expression of five markers (glypican 3, GPC-3; lymphatic vessel endothelial hyaluronan receptor 1, LYVE-1; survivin; heat shock 70 kDa protein, HSP70; and glutamine synthetase, GS), known to be differentially expressed between dysplastic nodule and well-differentiated HCC,[20,21] to clarify if the molecular alterations in early-stage hepatocarcinogenesis can be detected differentially in EOB-AFP class A, B, and C HCCs. IHC analysis suggested no differential expression of LYVE-1, survivin, and HSP70 among the EOB-AFP classes (data not shown). Interestingly, GS was most abundantly expressed in class A HCCs, and its expression was relatively decreased in class B and C HCCs with borderline significance ($P = 0.06$) (Fig. S3A,B). In contrast, GPC-3 expression was highest in class C HCCs and relatively decreased in class A and B HCCs with statistical significance ($P = 0.03$). We investigated the microarray data of 238 independent HCC cases and validated the positive correlation between *OATP1B3* and *GLUL* (encoding GS) and the weak negative correlation between *OATP1B3* and *GPC3* (encoding GPC-3).

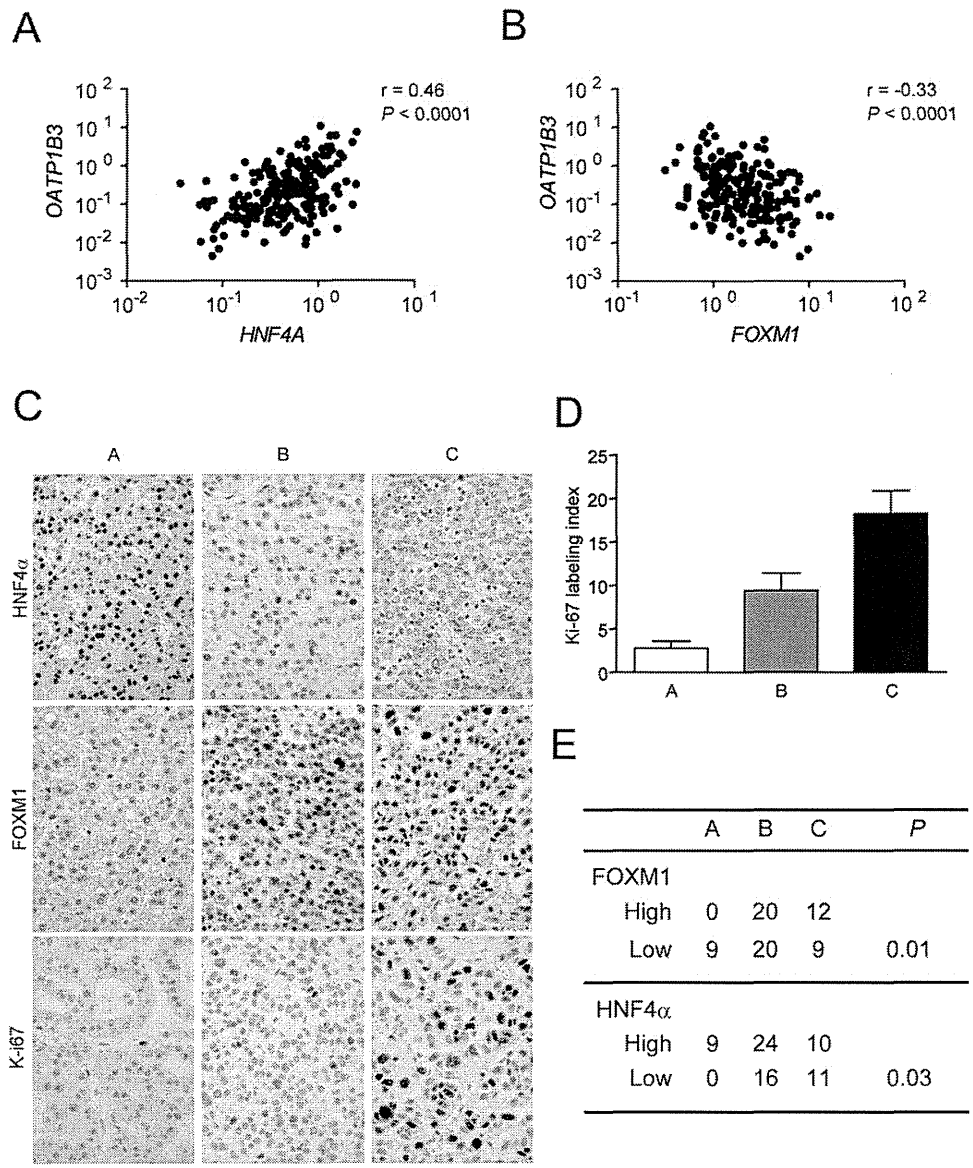

E

	A	B	C	P
FOXM1				
High	0	20	12	
Low	9	20	9	0.01
HNF4α				
High	9	24	10	
Low	0	16	11	0.03

Fig. 2. Transcriptional programs of HCCs corresponding to the EOB-MRI findings and serum AFP. (A,B) Scatterplot analyses of the microarray data of 238 HCCs. (C) Representative photomicrographs of IHC staining with anti-HNF4α, anti-FOXM1, and anti-Ki-67 antibodies in class A, B, and C HCCs, according to the EOB-AFP classification. (D) Ki-67 labeling index in class A, B, and C HCCs. (E) Summary of FOXM1 and HNF4α expression in class A, B, and C HCCs.

Regulation of Gd-EOB-DTPA Uptake and Tumorigenic Capacity by HNF4α in Hyperintense HCC. Microarray and IHC analyses suggested the activation of transcription factor HNF4α in hyperintense HCC, but its role in the maintenance of hepatocyte function and Gd-EOB-DTPA uptake has not yet been clarified. To directly explore the role of HNF4α in Gd-EOB-DTPA uptake and tumorigenic capacities, we transplanted tumor cells from hyper- and hypointense primary HCC specimens into NOD/SCID mice (Fig. 3A). We confirmed on EOB-MRI that Gd-EOB-DTPA uptake capacity was relatively maintained in the secondary xenotransplanted tumors that developed in the subcutaneous lesions of the mice (Fig. 3B).

Using a retrovirus system *in vitro*, we then introduced shRNA targeting *HNF4A* (Sh-HNF4A) or scramble (Sh-Scr) into tumor cells obtained from a hyperintense HCC. We confirmed the reduction of HNF4α protein expression in Sh-HNF4A-transfected cells compared with Sh-Scr-transfected cells by western blotting (Fig. 3C, left panel). Interestingly, *HNF4A* knockdown resulted in a modest increase in *AFP* and *FOXM1* expression and a dramatic decrease in *CYP3A4* and *OATP1B3* expression (Fig. 3C, right panel). It also resulted in the loss of OATP1B3 protein expression, and striking morphological changes were confirmed by immunofluorescence and phase-contrast microscopy (Fig. 3D). Sh-HNF4A-transfected cells displayed long, thin cell shapes with neurite-like extensions, whereas Sh-Scr-transfected cells were relatively smooth and round. Sh-Scr- or Sh-HNF4A-transfected cells were further injected subcutaneously into NOD/SCID mice, and aggressive tumor growth accompanied with the loss of Gd-EOB-DTPA uptake capacity was

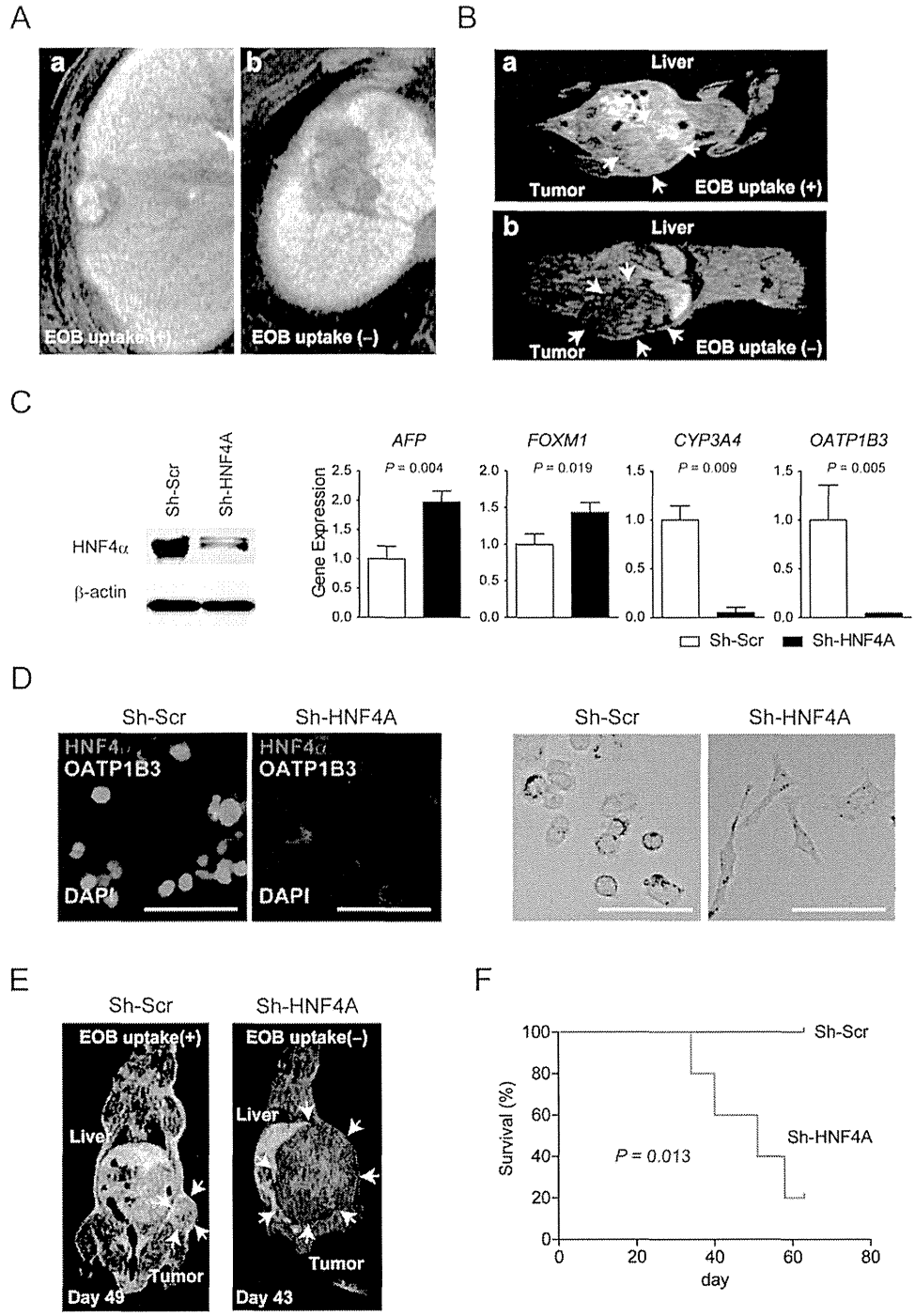

Fig. 3. HNF4α regulates a mature hepatocyte-like, less aggressive HCC phenotype coupled with Gd-EOB-DTPA uptake in hyperintense HCC. (A) MRI scans of hyperintense (a) and hypointense (b) HCCs in the hepatobiliary phase before surgery. The T/N signal intensity ratios of the images in the hepatobiliary phase were 1.02 (left panel) and 0.49 (right panel). Surgically resected specimens were subsequently used for mouse xenotransplantation. (B) MRI scans of NOD/SCID mouse xenotransplanted with hyperintense (a) and hypointense (b) HCCs in the hepatobiliary phase. The T/N signal intensity ratios of the images were 0.82 (upper panel) and 0.45 (lower panel). (C) Left panel: Expression of HNF4α protein by western blotting. Hyperintense HCC cells were harvested in dishes and treated with retroviruses encoding an expression cassette against *HNF4A* (Sh-HNF4A) or scramble sequence (Sh-Scr). Right panel: qRT-PCR of *AFP, FOXM1, CYP3A4*, and *OATP1B3* in hyperintense HCC cells transfected with Sh-Scr or Sh-HNF4A. (D) Left panel: Immunofluorescence analysis of HNF4α (red) and OATP1B3 (green) in hyperintense HCC cells transfected with Sh-Scr or Sh-HNF4A (scale bar = 100 μm). Right panel: Representative photomicrographs of hyperintense HCC cells transfected with Sh-Scr or Sh-HNF4A (scale bar = 100 μm). (E) MRI scans of NOD/SCID mouse xenotransplanted with hyperintense HCC cells transfected with Sh-Scr (day 49 after transplantation) or Sh-HNF4A (day 43 after transplantation). The T/N signal intensity ratios of the images in the hepatobiliary phase were 0.65 (left panel) and 0.34 (right panel). (F) Survival of NOD/SCID mice xenotransplanted with hyperintense HCC cells transfected with Sh-Scr (n = 5) or Sh-HNF4A (n = 5).

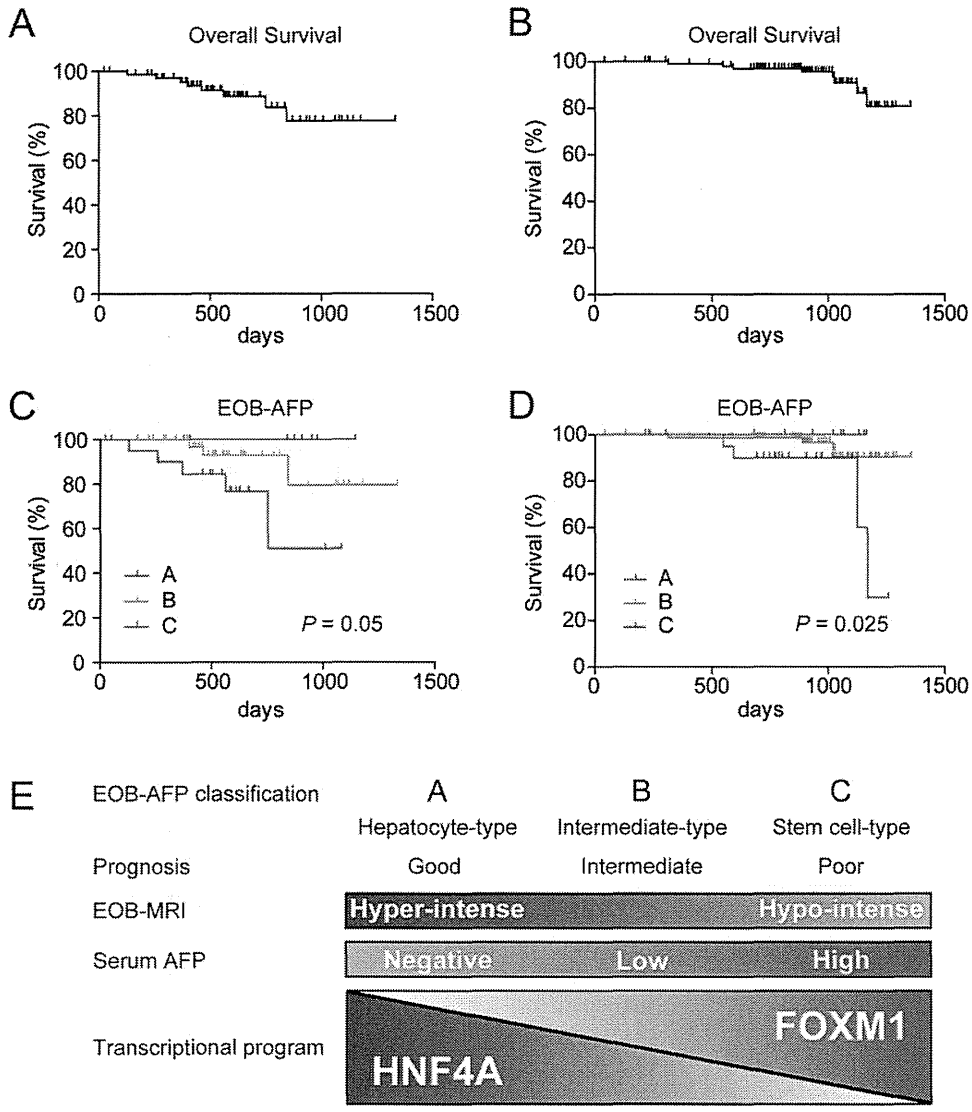

Fig. 4. Prognostic utility of the EOB-AFP classification. (A,B) Overall survival curves of Cohorts 1 (A) and 2 (B). (C,D) Overall survival curves of Cohorts 1 (C) and 2 (D) according to the EOB-AFP classification. (E) The EOB-AFP classification system and its molecular basis.

observed in Sh-HNF4A-transfected cells, whereas Sh-Scr-transfected cells still showed Gd-EOB-DTPA uptake with less tumorigenic capacity (Fig. 3E). Mice xenotransplanted with Sh-HNF4A-transfected cells had a worse prognosis compared with those xenotransplanted with Sh-Scr-transfected cells (Fig. 3F), indicating a crucial role for HNF4α in the maintenance of a mature hepatocyte-like, less aggressive HCC phenotype coupled with Gd-EOB-DTPA uptake capacity.

Prognosis of Early-Stage HCC by EOB-AFP Classification. Finally, we evaluated the prognosis of patients with HCC diagnosed by EOB-MRI and serum AFP. To exclude the potential effect of lead-time bias on survival analysis for HCCs at different stages, we evaluated the power of the EOB-AFP classification system to predict the prognosis of patients with early-stage BCLC stage 0 or A HCCs diagnosed by EOB-MRI in an independent multicenter cohort (Cohort 2). Nine of the 109 HCC cases (8.3%) were diagnosed with hyperintense HCCs and were found to be significantly associated with low serum AFP levels (Table 1). The clinicopathologic characteristics of the patients defined by the EOB-AFP classification are shown in Supporting Table 5. The median follow-up times in Cohorts 1 and 2 were 569 and 932 days, respectively. The 3-year overall survival rates in Cohorts 1 and 2 were 77.7% and 90.9%, respectively (Fig. 4A,B). The prognosis of HCC patients was not separated by TNM or BCLC stages because most of these patients were diagnosed at early stages (Fig. S4A-D); nevertheless, the EOB-AFP classification system robustly stratified HCCs according to survival with statistically significant differences between the classes (Fig. 4C,D). EOB-AFP class A patients had 100% overall survival, whereas class C patients had 30% overall survival at 1,200 days after radical resection in Cohort 2.

The prognosis of HCC patients stratified by the EOB-AFP classification was most likely affected by the malignant nature of the tumor at surgical resection, because EOB-AFP class C patients showed a 40-60% recurrence-free survival rate, whereas class A patients had a 88-100% recurrence-free survival rate at 1 year after radical resection in both cohorts (Fig. S5).

Altogether, our data, for the first time, revealed that the prognosis of early-stage HCC patients is heterogeneous and related to the malignant phenotypes of the tumors, even after successful treatment by radical resection. The EOB-AFP classification system reflects the malignant nature of the tumor and predicts the survival of early-stage HCC patients prior to surgery.

Discussion

Among several HCC staging systems currently used,[2] the BCLC system is recommended because it is linked to treatment strategy.[22] The assessment of the malignant nature of tumors coupled with current staging systems will supplement the management of early-stage HCC[23] because early recurrence after potentially curative treatment may be associated with the characteristics of the resected tumor rather than the development of a *de novo* HCC in the background liver.[24] Molecular profiling approaches have tried to evaluate the malignant features of HCCs and the surrounding noncancerous liver tissue,[3-6,12,18] although the evaluation of the potential clinical application of these approaches is ongoing. Our EOB-AFP classification system is molecularly related to the *OATP1B3* gene signature, which can be used to classify HCCs according to their stem/maturational status. Interestingly, the differential expression of *OATP1B3* was also noted in two HCC subtypes associated with the stem/maturational status, as reported recently by our group (hepatic stem cell-like and mature hepatocyte-like HCC)[12] and others (hepatoblast-type and hepatocyte type)[4] (Fig. S6). As expected, all class A HCCs were categorized as mature hepatocyte-like HCC in Cohort 1 (data not shown). The stem/maturational status defined by the EOB-AFP classification is most likely regulated by at least two transcription factors: HNF4α and FOXM1 (Fig. 4E).

HNF4α was first discovered as a liver-enriched nuclear orphan receptor activating the transcription of transthyretin genes, and it is known to regulate bile acid and cholesterol metabolism.[25] The liver-specific loss of *HNF4A* in adult mice results in hepatocyte proliferation,[26] whereas the introduction of *HNF4A* suppresses HCC growth.[27,28] Furthermore, a recent study suggested a role for *HNF4A* as a tumor suppressor in inflammation-related hepatocarcinogenesis through the regulation of microRNAs.[29] The present study demonstrated a crucial role for HNF4α in maintaining a hepatocyte-like, less aggressive phenotype coupled with Gd-EOB-DTPA uptake in a class A HCC by directly modifying *HNF4A* gene expression. Thus, *HNF4A* may work as a tumor suppressor gene and inhibit the progression of HCC, which may be related to the good prognosis of class A HCCs.

FOXM1 belongs to the forkhead superfamily of transcription factors and regulates a myriad of biologic processes including cell proliferation and differentiation.[30] The pivotal role of FOXM1 in liver development and regeneration has been reported previously.[17] FOXM1 was also required for HCC development in a mouse hepatocarcinogenesis model[31] and acted as an oncogene in a transgenic mouse model.[32] It was recently shown that FOXM1 levels are elevated in various cancers including HCC.[32,33] A prognostic role for FOXM1 in HCC patients after liver transplantation was also reported[34]; this may be associated with the metastatic capacity of tumors regulated by FOXM1.[35] As FOXM1 and AFP are known to be activated during liver regeneration and hepatocarcinogenesis, serum AFP levels may be a surrogate marker for the expression status of FOXM1 and thus facilitate the prognostic stratification of HCCs by the EOB-AFP classification.

Among the molecular markers reported to be differentially expressed between dysplastic nodule and well-differentiated HCC, we found preferential overexpression of GS in EOB-AFP class A and GPC-3 in class C HCCs. Our data suggest that class A and class C HCCs may follow different processes of early hepatocarcinogenesis events that might be associated with the differential activation of HNF4α and FOXM1, and further studies are required to obtain molecular insights into these processes.

Our overall survival data in Cohort 2 indicated that EOB-AFP class A patients had 100% overall survival, whereas class C patients had 30% overall survival at 1,200 days after radical resection. This suggests that the micro-dissemination of tumor cells in EOB-AFP class C HCC patients has already occurred by the time they are diagnosed with early-stage disease. Indeed, 50% of all class C patients showed tumor recurrence, whereas 88-100% of class A patients showed no recurrence within 1 year of resection; this is consistent with a recent study evaluating the clinical features of hyperintense HCCs[36] and may be due to